Progress In Electromagnetics Research, Vol. 146, 57–69, 2014

RCS Reduction of Open-Ended Circular Waveguide Cavity with Corrugations Using Mode Matching and Scattering Matrix Analysis

Young Dam Kim*, Ho Lim, Jung Hoon Han, Won Young Song, and Noh Hoon Myung

Abstract—A scattered radar signal by a jet engine inlet involves engine information of the target. The jet engine RCS due to the engine inlet is therefore significant in radar target recognition. Accordingly, several accurate analyses of the jet engine RCS have been reported. Reduction of the jet engine RCS is also required for stealth technology. We suggest a new approach for jet engine RCS reduction that involves the insertion of many small corrugations into the jet engine inlet. The proposed jet engine structure is assumed to be a circular waveguide cavity with many corrugations. The structure is analyzed by combining a mode matching technique with a scattering matrix analysis. The proposed closed-form RCS solutions of the corrugated engine structure are validated with a MoM simulation using FEKO. The proposed closed-form solution has numerical efficiency and rapid convergence. Using the characteristics of the solution, we simply apply a genetic algorithm (GA) to optimize the structure of the corrugations in terms of minimizing the RCS.

1. INTRODUCTION

The radar cross section (RCS) of a jet engine is important in that it plays a key role in radar target recognition. If a transmitted radar signal is scattered from the interior of the jet engine, the radar signal is modulated by rotating jet engine blades. The modulated signal referred to jet engine modulation (JEM) provides significant information, such as the spool rate, blade length and blade number. By interpreting the JEM signal, enemy troops are able to identify the fighter type [1]. Reduction of the jet engine RCS is therefore important for stealth technology. For this reason, the jet engine RCS has been extensively studied in many electromagnetic problems.

Three remarkable methods to analyze jet engine RCS have been reported. The first is an exact solution using a mode matching method with a scattering matrix analysis [2–6]. In this method, the jet engine is treated as a complex open-ended waveguide cavity structure. In order to analyze a structure that has some obstacles, the scattering matrix method applies a modal analysis to each simple distinct section composing the complex waveguide cavity structure. A scattering property of the entire structure, represented in matrix form, is attained by cascading the modal coefficients of all sections. The second is an asymptotic solution using high-frequency methods such as shooting and bouncing rays (SBR) [7], geometrical theory of diffraction (GTD) [8], physical optics (PO) [9] and generalized ray expansion (GRE) [10]. Because the size of jet engine is typically much larger than the wavelength and these methods rely on the ray tracing method, they have good applicability to arbitrary and large structures. The third is a hybrid solution combining an integral or differential of Maxwell equations with the two methods described above [11–14]. The mode matching method or high-frequency method is utilized for the front part of the jet engine due to its simple structure. Low-frequency methods using Maxwell's integral equations or differential equations are applied to the end part of the jet engine which has

Received 28 February 2014, Accepted 1 April 2014, Scheduled 23 April 2014

* Corresponding author: Young Dam Kim (hohohahe@kaist.ac.kr).

The authors are with the Department of Electrical Engineering, Korea Advanced Institute of Science and Technology (KAIST), 291 Daehak-ro, Yuseong-gu, Daejon 305-701, Republic of Korea.

complex jet engine blades. By combining two methods, both computational efficiency in the front part and solution accuracy in the end part are attainable.

Reduction of the jet engine RCS has been researched via two methods. The first is geometrical modification of the jet engine structure, which backscatters incident radar waves to the opposite direction of the incidence. For reduction of the jet engine RCS, the straight jet engine structure is commonly bent into an S-shape [6, 7]. This method is quite effective but the whole structure of the jet engine requires large modification relative to the straight jet engine. The second is using radar absorbing material (RAM) coating on the surface of the jet engine [8]. Although the RAM has a simple property of absorbing electromagnetic wave in the molecular level, large RCS reduction is attained by coating the RAM. In order to obtain a better effect, many RAMs that have different permittivity and permeability should be accumulated in a multilayered coating [15]. In the design of the multilayered coating, GA (Genetic Algorithm) optimization of the multilayered RAM brings a significant reduction of the RCS [16, 17]. However, this method is quite expensive with respect to material cost and maintenance.

In this paper, we suggest a new method for engine RCS reduction where a corrugated open-ended circular waveguide cavity is treated as the jet engine analysis model. Many small-sized corrugations compared to the size of the jet engine are inserted into the waveguide cavity. The inserted corrugations serve as a waveguide filter which suppresses surface current in the waveguide cavity, and the RCS of the jet engine is consequentially reduced. This method can feasibly be realized without modification of the whole engine structure, and it is also competitive in terms of cost and maintenance. In order to analyze the structure, we used a mode matching technique combined with a scattering matrix to obtain an analytic solution. To analyze the open-end of the structure, the mode-matching technique was reciprocally able to convert a closed form equation of both incident and scattering waves to matrices of the excited modal coefficients at the aperture [18]. For the complicated corrugations in the circular waveguide [19], many unit scattering matrices matching the unit circular waveguide as part of the whole corrugated waveguide were cascaded step by step [20]. Combining the mode matching and the scattering matrix solutions, a closed-form RCS solution was finally obtained. Since the final solution has the characteristics of a modal analysis, the solution rapidly converges and is numerically efficient. Using these two characteristics, we suggested a simple cost function for optimizing the corrugation structure. Applying the GA algorithm, we found an optimized corrugation design for minimizing RCS.

2. RCS ANALYSIS OF OPEN-ENDED CIRCULAR WAVEGUIDE CAVITY WITH CORRUGATIONS

2.1. Analysis Structure and Methods

The suggested model for the RCS reduction is illustrated in Figure 1. We assume the jet engine model as a large open-ended circular waveguide cavity. In order to reduce the RCS of the jet engine, small-sized corrugations are inserted into the waveguide.

Figure 2 shows divided regions of the open-ended circular waveguide with corrugations and describes

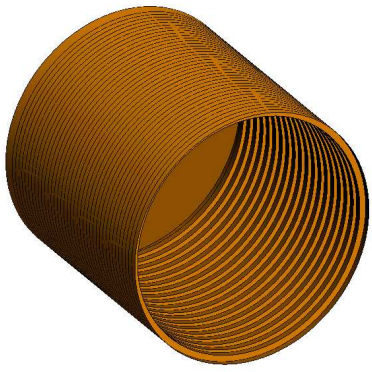

Figure 1. Open-ended circular waveguide cavity with corrugation.

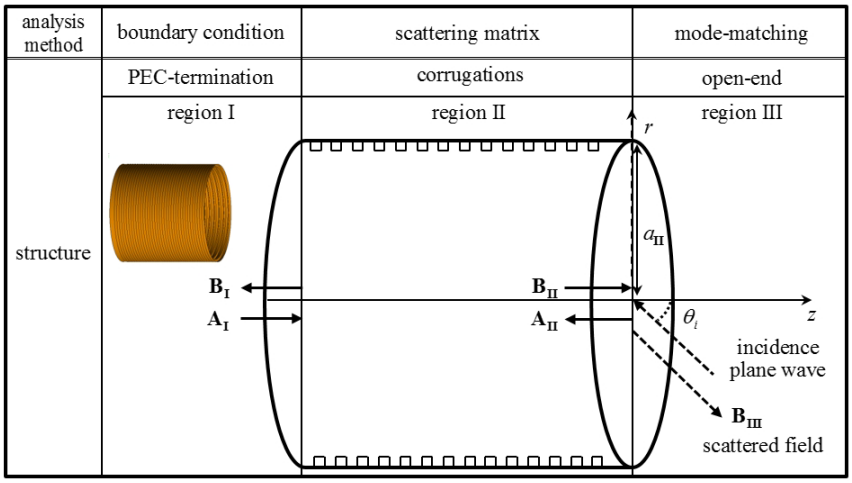

Figure 2. Divided structure with three regions corresponding to each analysis method.

the analysis method according to each region. The aperture of the analysis structure is orthogonal to the z axis, and the analysis structure is divided into three regions with respect to the analysis method, as shown in Figure 2. First, we used mode-matching at the open-ended aperture, and the obtained equations were transformed to matrix equations for connection with the scattering-matrix method. Second, the corrugations were divided into many simple sections, and the scattering matrix method was applied to each section. Cascading all sections, a scattering characteristic was obtained for all corrugations. Third, a boundary condition by perfect electric conductor (PEC) termination was simply applied. With the three conditions, the unknown coefficients of Fourier series and transform $\mathbf{A_I}$, $\mathbf{B_I}$, $\mathbf{A_{II}}$, $\mathbf{B_{II}}$ and $\mathbf{B_{III}}$ were obtained. Finally, the RCS of the analysis structure was evaluated.

2.2. Field Representation

We utilize normalized field equations for simplicity of the field expression in [19]. This normalization is equal to assign both ε and μ to unity. With $e^{-i\omega t}$ time convention, the field is given by

$$\bar{E} = \sqrt{\mu}\bar{E}' \quad \bar{H} = \sqrt{\mu}\bar{H}' \quad t = \sqrt{\mu\varepsilon}t' \tag{1}$$

Maxwell's equations for the normalized field expressions are as follows.

$$\nabla \times \bar{E}' = in\frac{\partial \bar{H}'}{\partial t'} \quad \nabla \times \bar{H}' = in\frac{\partial \bar{E}'}{\partial t'} \tag{2}$$

where n is the refractive index of the medium. The electric and magnetic fields are expressed with combination of electric and magnetic Hertz potentials such that

$$\bar{E}' = \nabla \times \nabla \times \bar{\Pi}_m + \omega' n \nabla \times \bar{\Pi}_e \tag{3}$$

$$\bar{H}' = \nabla \times \nabla \times \bar{\Pi}_e + \omega' n \nabla \times \bar{\Pi}_m \tag{4}$$

where $\bar{\Pi}_m$ and $\bar{\Pi}_e$ are the magnetic Hertz potential and the electric Hertz potential, respectively. In regions I and II (the corrugated circular waveguide), the tangential fields with respect to the waveguide aperture are represented as

$$\bar{E}_{\mathbf{I}} = \sum_{v=-\infty}^{\infty}\sum_{u=1}^{2N_{\mathbf{I}}}\left[\mathbf{A}_{\mathbf{I}}^{(v)}(u)e^{ik_{vu}^{\mathbf{I}}z} + \mathbf{B}_{\mathbf{I}}^{(v)}(u)e^{-ik_{vu}^{\mathbf{I}}z}\right]\bar{\mathbf{e}}_{\mathbf{I}}^{(v)}(u) \tag{5}$$

$$\bar{H}_{\mathbf{I}} = \sum_{v=-\infty}^{\infty}\sum_{u=1}^{2N_{\mathbf{I}}}\left[\mathbf{A}_{\mathbf{I}}^{(v)}(u)e^{ik_{vu}^{\mathbf{I}}z} - \mathbf{B}_{\mathbf{I}}^{(v)}(u)e^{-ik_{vu}^{\mathbf{I}}z}\right]\bar{\mathbf{h}}_{\mathbf{I}}^{(v)}(u) \tag{6}$$

$$\bar{E}_{\mathbf{II}} = \sum_{v=-\infty}^{\infty}\sum_{u=1}^{2N_{\mathbf{II}}}\left[\mathbf{A}_{\mathbf{II}}^{(v)}(u)e^{-ik_{vu}^{\mathbf{II}}z} + \mathbf{B}_{\mathbf{II}}^{(v)}(u)e^{ik_{vu}^{\mathbf{II}}z}\right]\bar{\mathbf{e}}_{\mathbf{II}}^{(v)}(u) \tag{7}$$

$$\bar{H}_{\mathbf{II}} = \sum_{v=-\infty}^{\infty}\sum_{u=1}^{2N_{\mathbf{II}}}\left[-\mathbf{A}_{\mathbf{II}}^{(v)}(u)e^{-ik_{vu}^{\mathbf{II}}z} + \mathbf{B}_{\mathbf{II}}^{(v)}(u)e^{ik_{vu}^{\mathbf{II}}z}\right]\bar{\mathbf{h}}_{\mathbf{II}}^{(v)}(u) \tag{8}$$

where the unknown modal coefficients of the Fourier series are defined as

$$\mathbf{A}_{\mathbf{I,II}}^{(v)} = \left[A_m^{\mathbf{I,II}(v)}(1),\ldots,A_m^{\mathbf{I,II}(v)}(N_{\mathbf{I,II}}),A_e^{\mathbf{I,II}(v)}(1),\ldots,A_e^{\mathbf{I,II}(v)}(N_{\mathbf{I,II}})\right]^T \tag{9}$$

$$\mathbf{B}_{\mathbf{I,II}}^{(v)} = \left[B_m^{\mathbf{I,II}(v)}(1),\ldots,B_m^{\mathbf{I,II}(v)}(N_{\mathbf{I,II}}),B_e^{\mathbf{I,II}(v)}(1),\ldots,B_e^{\mathbf{I,II}(v)}(N_{\mathbf{I,II}})\right]^T \tag{10}$$

and

$$\bar{\mathbf{e}}_{\mathbf{I,II}}^{(v)} = \left[\bar{e}_m^{\mathbf{I,II}(v)}(1),\ldots,\bar{e}_m^{\mathbf{I,II}(v)}(N_{\mathbf{I,II}}),\bar{e}_e^{\mathbf{I,II}(v)}(1)\ldots,\bar{e}_e^{\mathbf{I,II}(v)}(N_{\mathbf{I,II}})\right]^T \tag{11}$$

$$\bar{\mathbf{h}}_{\mathbf{I,II}}^{(v)} = \left[\bar{h}_m^{\mathbf{I,II}(v)}(1),\ldots,\bar{h}_m^{\mathbf{I,II}(v)}(N_{\mathbf{I,II}}),\quad \bar{h}_e^{\mathbf{I,II}(v)}(1),\ldots,\bar{h}_e^{\mathbf{I,II}(v)}(N_{\mathbf{I,II}})\right]^T \tag{12}$$

$$\bar{e}_m^{\mathbf{I,II}(v)} = i\beta_{vn}^{\mathbf{I,II}}\nabla\bar{\Pi}_m^{\mathbf{I,II}},\quad \bar{e}_e^{\mathbf{I,II}(v)} = \omega n_{\mathbf{I,II}}\nabla\bar{\Pi}_e^{\mathbf{I,II}}\times\hat{z} \tag{13}$$

$$\bar{h}_m^{\mathbf{I,II}(v)} = \omega n_{\mathbf{I,II}}\nabla\bar{\Pi}_m^{\mathbf{I}}\times\hat{z},\quad \bar{h}_e^{\mathbf{I,II}(v)} = i\beta'^{\mathbf{I,II}}_{vn}\nabla\bar{\Pi}_e^{\mathbf{I,II}} \tag{14}$$

$$\bar{\Pi}_m^{\mathbf{I,II}(v)} = e^{iv\phi}J_v\left(\frac{\chi_{vn}}{a_{\mathbf{I,II}}}r\right),\quad \bar{\Pi}_e^{\mathbf{I,II}(v)} = e^{iv\phi}J_v\left(\frac{\chi'_{vn}}{a_{\mathbf{I,II}}}r\right) \tag{15}$$

$$\bar{e}_m^{\mathbf{I,II}(v)}(u) = i\beta_{vu}^{\mathbf{I,II}}\left[\hat{r}e^{iv\phi}\frac{\chi_{\nu u}}{a_{\mathbf{I,II}}}J'_\nu\left(\frac{\chi_{\nu u}}{a_{\mathbf{I,II}}}r\right) + \hat{\phi}\frac{1}{r}i\nu e^{iv\phi}J_\nu\left(\frac{\chi_{\nu u}}{a_{\mathbf{I,II}}}r\right)\right] \tag{16}$$

$$\bar{e}_e^{\mathbf{I,II}(v)}(u) = \omega n_{\mathbf{II}}\left[\hat{r}\frac{1}{r}i\nu e^{iv\phi}J_\nu\left(\frac{\chi'_{\nu u}}{a_{\mathbf{I,II}}}r\right) - \hat{\phi}e^{iv\phi}\frac{\chi'_{\nu u}}{a_{\mathbf{I,II}}}J'_\nu\left(\frac{\chi'_{\nu u}}{a_{\mathbf{I,II}}}r\right)\right] \tag{17}$$

$$\bar{h}_m^{\mathbf{I,II}(v)}(u) = \omega n_{\mathbf{II}}\left[\hat{r}\frac{1}{r}i\nu e^{iv\phi}J_\nu\left(\frac{\chi_{\nu u}}{a_{\mathbf{I,II}}}r\right) - \hat{\phi}e^{iv\phi}\frac{\chi_{\nu u}}{a_{\mathbf{I,II}}}J'_\nu\left(\frac{\chi_{\nu u}}{a_{\mathbf{I,II}}}r\right)\right] \tag{18}$$

$$\bar{h}_e^{\mathbf{I,II}(v)}(u) = i\beta'^{\mathbf{I,II}}_{vu}\left[\hat{r}e^{iv\phi}\frac{\chi'_{\nu u}}{a_{\mathbf{I,II}}}J'_\nu\left(\frac{\chi'_{\nu u}}{a_{\mathbf{I,II}}}r\right) + \hat{\phi}i\nu e^{iv\phi}J_\nu\left(\frac{\chi'_{\nu u}}{a_{\mathbf{I,II}}}r\right)\right]a. \tag{19}$$

Note that $J_v(\cdot)$ is the Bessel function of the first kind and order v, and $J'_v(\cdot)$ denotes differentiation with respect to the argument. χ_{vu} is defined as the uth root of the v-order Bessel function $J_v(\cdot)$ and χ'_{vu} is defined as the uth root of the derivative of the v-order Bessel function $J'_v(\cdot)$. a is the radius of the aperture in the relevant region. $\hat{r}$ and $\hat{\phi}$ denote unit vectors in cylindrical coordinates. Propagation constant for the transverse magnetic (TM) mode and transverse electric (TE) mode (magnetic Hertz potential and electric Hertz potential) are respectively represented as

$$k_{vu}^{\mathbf{I,II}} = \begin{cases}\beta_{vu}^{\mathbf{I,II}} = \sqrt{(\omega n_{\mathbf{I,II}})^2 - \left(\frac{\chi_{vu}}{a_{\mathbf{I,II}}}\right)^2}\\ \beta'^{\mathbf{I,II}}_{vu} = \sqrt{(\omega n_{\mathbf{I,II}})^2 - \left(\frac{\chi'_{vu}}{a_{\mathbf{I,II}}}\right)^2}\end{cases}. \tag{20}$$

In the region III (the open-ended region) the outer scattered fields by the inlet of the waveguide are represented as

$$\bar{E}_{\mathbf{III}} = \sum_{v=-\infty}^{\infty}\int_0^\infty \mathbf{B}_{\mathbf{III}}^{(v)}(\zeta)e^{i\kappa z}\bar{\mathbf{e}}_{\mathbf{III}}^{(v)}(\zeta)d\zeta \tag{21}$$

$$\bar{H}_{\mathbf{III}} = \sum_{v=-\infty}^{\infty}\int_0^\infty \mathbf{B}_{\mathbf{III}}^{(v)}(\zeta)e^{i\kappa z}\bar{\mathbf{h}}_{\mathbf{III}}^{(v)}(\zeta)d\zeta \tag{22}$$

where $\mathbf{B}_{\mathbf{III}}^{(v)}(\zeta)$ is the unknown spectral coefficient of the Fourier transform and

$$\bar{\mathbf{e}}_{\mathbf{III}}^{(v)}(\zeta) = \left[\bar{e}_m^{\mathbf{III}(v)}(\zeta)\,\bar{e}_e^{\mathbf{III}(v)}(\zeta)\right]^T \tag{23}$$

$$\bar{\mathbf{h}}_{\mathbf{III}}^{(v)}(\zeta) = \left[\bar{h}_m^{\mathbf{III}(v)}(\zeta)\,\bar{h}_e^{\mathbf{III}(v)}(\zeta)\right]^T \tag{24}$$

$$\bar{e}_m^{\mathbf{III}(v)} = i\kappa\nabla\bar{\Pi}_m^{\mathbf{III}}, \quad \bar{e}_e^{\mathbf{III}(v)} = \omega n_{\mathbf{III}}\nabla\bar{\Pi}_e^{\mathbf{III}} \times \hat{z} \tag{25}$$

$$\bar{h}_m^{\mathbf{III}(v)} = \omega n_{\mathbf{III}}\nabla\bar{\Pi}_m^{\mathbf{III}} \times \hat{z}, \quad \bar{h}_e^{\mathbf{III}(v)} = i\kappa\nabla\bar{\Pi}_e^{\mathbf{III}} \tag{26}$$

$$\bar{\Pi}_m^{\mathbf{III}(v)} = \bar{\Pi}_e^{\mathbf{III}(v)} = e^{iv\phi}J_v(\zeta r) \tag{27}$$

$$\kappa = \sqrt{(\omega n_{\mathbf{III}})^2 - \zeta^2} \tag{28}$$

$$\bar{e}_m^{\mathbf{III}(v)}(\zeta) = i\kappa\left[\hat{r}e^{iv\phi}\zeta J_\nu'(\zeta r) + \hat{\phi}\frac{1}{r}ive^{iv\phi}J_\nu(\zeta r)\right] \tag{29}$$

$$\bar{e}_e^{\mathbf{III}(v)}(\zeta) = \omega n_{\mathbf{III}}\left[\hat{r}\frac{1}{r}ive^{iv\phi}J_\nu(\zeta r) - \hat{\phi}e^{iv\phi}\zeta J_\nu'(\zeta r)\right] \tag{30}$$

$$\bar{h}_m^{\mathbf{III}(v)}(\zeta) = \omega n_{\mathbf{III}}\left[\hat{r}\frac{1}{r}ive^{iv\phi}J_\nu(\zeta r) - \hat{\phi}e^{iv\phi}\zeta J_\nu'(\zeta r)\right] \tag{31}$$

$$\bar{h}_e^{\mathbf{III}(v)}(\zeta) = i\kappa\left[\hat{r}e^{iv\phi}\zeta J_\nu'(\zeta r) + \hat{\phi}\frac{1}{r}ive^{iv\phi}J_\nu(\zeta r)\right]. \tag{32}$$

We assume that the incidence plane wave impinges with the angle θ_i, as shown in Figure 2. For convenience of offsetting in the calculation, we set arbitrary fields reflected by a virtual PEC plate, and these fields are satisfied with the law of reflection. Although the offsetting only provides a valid θ_i range from 0° to 50°, the range is sufficient to observe scattering effect by the jet engine inlet because the significant JEM emerges around the normal axis of the jet engine aperture ($\theta_i = 0°$). The two pairs of the incidence and reflected plane wave according to the TM and TE polarization are represented as

$$\left(\bar{H}^i\right)_{\mathrm{TM}} = \hat{y}e^{ikx\sin\theta_i + ikz\cos\theta_i} = \hat{y}e^{-ikz\cos\theta_i}\sum_{v=-\infty}^{\infty} i^v J_v(kr\sin\theta_i)\, e^{iv\phi} \tag{33}$$

$$\left(\bar{H}^r\right)_{\mathrm{TM}} = \hat{y}e^{ikx\sin\theta_i - ikz\cos\theta_i} = \hat{y}e^{-ikz\cos\theta_i}\sum_{v=-\infty}^{\infty} i^v J_v(kr\sin\theta_i)\, e^{iv\phi} \tag{34}$$

$$\left(\bar{E}^i\right)_{\mathrm{TE}} = \hat{y}e^{ikx\sin\theta_i - ikz\cos\theta_i} = \hat{y}e^{-ikz\cos\theta_i}\sum_{v=-\infty}^{\infty} i^v J_v(kr\sin\theta_i)\, e^{iv\phi} \tag{35}$$

$$\left(\bar{E}^r\right)_{\mathrm{TE}} = -\hat{y}e^{ikx\sin\theta_i + ikz\cos\theta_i} = -\hat{y}e^{ikz\cos\theta_i}\sum_{v=-\infty}^{\infty} i^v J_v(kr\sin\theta_i)\, e^{iv\phi} \tag{36}$$

2.3. Mode Matching and Scattering Matrix Analysis

The incidence plane wave is represented as the sum of the Bessel function of the first kind, represented as v. The entire fields are also represented in the same manner. Boundary conditions for the entire fields are then individually valid with respect to the arbitrary v. Therefore, the final solution can be obtained by superposition in terms of v. For an arbitrary v, tangential electric field continuity at the aperture requires

$$\bar{E}_{\mathbf{II}}^{(v)} = \bar{E}_{\mathbf{III}}^{(v)} + \left(\bar{E}^i + \bar{E}^r\right)_{\mathrm{TM,TE}}^{(v)} \tag{37}$$

For convenience, we apply power orthogonality described in [21] to (37), and the equations are represented as (A1). In order to connect mode-matching equations with scattering matrix, the equations are transformed into a matrix form such as

$$\mathbf{B}_{\mathbf{III}}^{(v)}(\zeta) = \left(Q_o^{(v)}\right)^{-1} P_o^{(v)}\left(\mathbf{A}_{\mathbf{II}}^{(v)} + \mathbf{B}_{\mathbf{II}}^{(v)}\right) \tag{38}$$

where $Q_o^{(v)}$ and $P_o^{(v)}$ are represented as (A3) and (A4), respectively. In the same manner, the tangential magnetic field continuity at the aperture requires

$$\bar{H}_{\mathbf{II}}^{(v)} = \bar{H}_{\mathbf{III}}^{(v)} + \left(\bar{H}^i + \bar{H}^r\right)_{\mathrm{TM,TE}}^{(v)} \tag{39}$$

The equation applied power orthogonality to (39) is represented as (A2), and the matrix form equation yields

$$R_o^{(v)}\left(\mathbf{B}_{\mathbf{II}}^{(v)}-\mathbf{A}_{\mathbf{II}}^{(v)}\right)=-\int_0^{\infty}\left(P_o^{(v)}\right)^H B_{\mathbf{III}}^{(v)}(\zeta)d\zeta+\mathbf{V}_{\mathrm{TE,TM}}^{(v)} \tag{40}$$

where $R_o^{(v)}$ and $\mathbf{V}_{\mathrm{TE,TM}}^{(v)}$ are represented as (A5) and (A6) respectively. Substituting (38) into (40), we obtain

$$R_o^{(v)}\left(\mathbf{B}_{\mathbf{II}}^{(v)}-\mathbf{A}_{\mathbf{II}}^{(v)}\right)=-X^{(v)}\left(\mathbf{A}_{\mathbf{II}}^{(v)}+\mathbf{B}_{\mathbf{II}}^{(v)}\right)+\mathbf{V}_{\mathrm{TE,TM}}^{(v)} \tag{41}$$

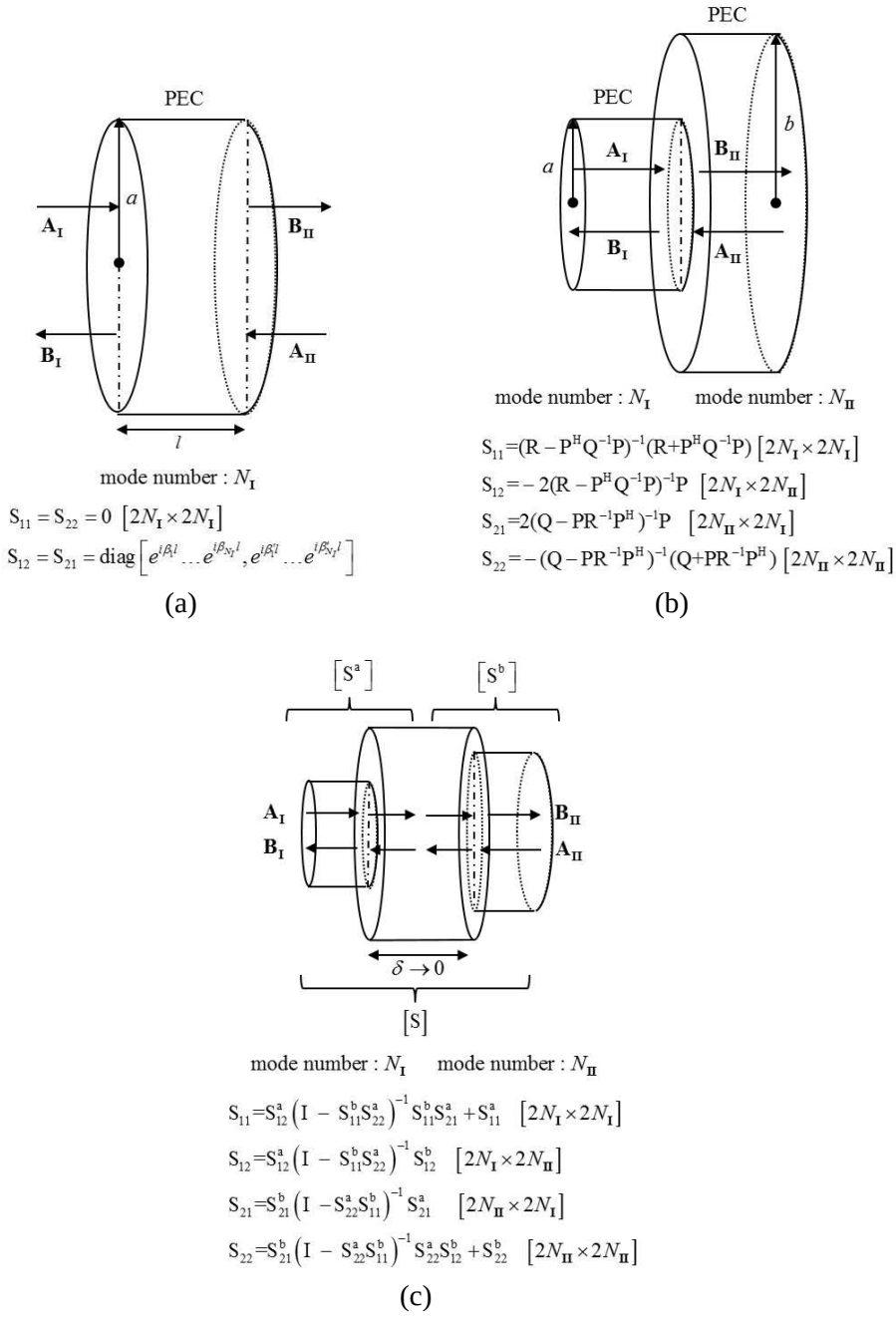

Figure 3. Scattering matrix method (a) continuous structure, and (b) discontinuous structure, and (c) cascading method between two structures.

where

$$X^{(v)} = \int_0^\infty \left(P_o^{(v)}\right)^H \left(Q_o^{(v)}\right)^{-1} P_o^{(v)} d\zeta. \tag{42}$$

$X^{(v)}$ is represented as (A7), and the integrals in the $X^{(v)}$ are numerically evaluated by the adaptive Gauss-Kronrod quadrature method in [22].

It is necessary to obtain another condition by using the scattering matrix of the corrugations with the boundary condition of the PEC-termination. The PEC boundary condition is simply expressed as $\mathbf{B}_{\mathbf{I}}^{(v)} = -\mathbf{A}_{\mathbf{I}}^{(v)}$. We then obtain

$$\mathbf{B}_{\mathbf{II}}^{(v)} = \left(S_{22}^{(v)} - S_{21}^{(v)} \left(I + S_{11}^{(v)}\right)^{-1} S_{11}^{(v)}\right) \mathbf{A}_{\mathbf{II}}^{(v)} \tag{43}$$

where $S_{11}^{(v)}$, $S_{12}^{(v)}$, $S_{21}^{(v)}$ and $S_{22}^{(v)}$ are evaluated by using Figure 3 describing the scattering matrix method case by case. The three cases are a continuous structure, a discontinuous structure and a cascading method between two structures $\mathbf{A_I}$, $\mathbf{A_{II}}$, $\mathbf{B_I}$ and $\mathbf{B_{II}}$ are modal coefficient vectors of Fourier series representing electromagnetic fields in the waveguide. These vectors have relation as

$$\begin{bmatrix} \mathbf{B_I} \\ \mathbf{B_{II}} \end{bmatrix} = \begin{bmatrix} S_{11} & S_{12} \\ S_{21} & S_{22} \end{bmatrix} \begin{bmatrix} \mathbf{A_I} \\ \mathbf{A_{II}} \end{bmatrix}. \tag{44}$$

The P, Q and R matrices for calculating the scattering matrix are represented as (B1), (B2) and (B3) respectively.

Using both (41) and (43), the unknown modal coefficients at the aperture $\mathbf{A}_{\mathbf{II}}^{(v)} + \mathbf{B}_{\mathbf{II}}^{(v)}$ can be evaluated as

$$\mathbf{A}_{\mathbf{II}}^{(v)} + \mathbf{B}_{\mathbf{II}}^{(v)} = \left(\Psi^{(v)} + I\right) \left(R_o^{(v)} \left(\Psi^{(v)} - I\right) + X^{(v)} \left(\Psi^{(v)} + I\right)\right)^{-1} \mathbf{V}_{\mathrm{TE,TM}}^{(v)} \tag{45}$$

where

$$\Psi^{(v)} = \left(S_{22}^{(v)} - S_{21}^{(v)} \left(I + S_{11}^{(v)}\right)^{-1} S_{11}^{(v)}\right). \tag{46}$$

Defining $\mathbf{\Omega}_{\mathrm{TM,TE}}^{(v)} = \mathbf{A}_{\mathbf{II}}^{(v)} + \mathbf{B}_{\mathbf{II}}^{(v)}$ and $\mathbf{\Omega}_{\mathrm{TM,TE}}^{(v)} = [\mathbf{\Omega}_m^{(v)}\ \mathbf{\Omega}_e^{(v)}]_{\mathrm{TM,TE}}^T$, the unknown spectral coefficient of the scattering field $\mathbf{B}_{\mathbf{III}}^{(v)}(\zeta)$ is represented as

$$\mathbf{B}_{\mathbf{III}}^{(v)}(\zeta) = \left(Q_o^{(v)}\right)^{-1} P_o^{(v)} \mathbf{\Omega}_{\mathrm{TM,TE}}^{(v)} \tag{47}$$

2.4. Closed-Form RCS Solution

The scattered electric and magnetic fields are obtained by substituting (47) into (21) and (22), respectively. In the far field observation, the stationary phase method can be applied to the semi-infinite bounded integrals about ζ. The obtained fields with respect to the incidence polarization are then substituted into the definition of the RCS, represented as

$$\sigma_{\mathrm{TM}} = \lim_{r_s \to \infty} \left(4\pi r_s^2 \frac{|E_\theta|^2 + |E_\phi|^2}{|E_i|^2}\right), \quad \sigma_{\mathrm{TE}} = \lim_{r_s \to \infty} \left(4\pi r_s^2 \frac{|H_\theta|^2 + |H_\phi|^2}{|H_i|^2}\right). \tag{48}$$

Finally we can express the closed-form RCS solution of the analysis structure as

$$\sigma_{\mathrm{TM}} = 4\pi \left\{ \begin{array}{l} \left| \sum_{v=-\infty}^{\infty} \sum_{u=1}^{N_{\mathbf{II}}} e^{iv\phi} e^{-i\left(\frac{v}{2}\right)\pi} \left(\begin{array}{l} \mathbf{\Omega}_m^{(v)}(u)\, i\beta_{vu}\chi_{vu} \dfrac{k^2 \sin\theta_i \cos 2\theta_i J_v'(\chi_{vu})}{\left[(k\sin\theta_i)^2 - \left(\frac{\chi_{vu}}{a_{\mathbf{II}}}\right)^2\right]} \\ + \mathbf{\Omega}_e^{(v)}(u)\, \omega n_{\mathbf{II}}\, (iv)\, (\cot\theta_i - \sin\theta_i)\, J_v(\chi_{vu}') \end{array} \right) J_v\left(ka_{\mathbf{II}} \sin\theta_i\right) \right|^2 \\ + \left| \sum_{v=-\infty}^{\infty} \sum_{u=1}^{N_{\mathbf{II}}} e^{iv\phi} e^{-i\left(\frac{v}{2}\right)\pi} \left(\mathbf{\Omega}_e^{(v)}(n)\, \omega \frac{n_{\mathbf{II}}}{n_{\mathbf{III}}} \frac{\chi_{vu}'^2}{a_{\mathbf{II}}} \frac{(k\cos\theta_i) J_v(\chi_{vu}')}{\left[(k\sin\theta_i)^2 - \left(\frac{\chi_{vu}'}{a_{\mathbf{II}}}\right)^2\right]} \right) J_v'\left(ka_{\mathbf{II}} \sin\theta_i\right) \right|^2 \end{array} \right\} \tag{49}$$

$$\sigma_{\mathrm{TE}}=4\pi\left\{\left|\sum_{v=-\infty}^{\infty}\sum_{u=1}^{N_{\mathbf{II}}}e^{iv\phi}e^{-i\left(\frac{v}{2}\right)\pi}\mathbf{\Omega}_e^v\left(u\right)i\frac{n_{\mathbf{II}}}{n_{\mathbf{III}}}\frac{\chi'^2_{vu}}{a_{\mathbf{II}}}J_v(\chi'_{vu})\frac{\left(k^2\cos\theta_i\right)J'_v(ka_{\mathbf{II}}\sin\theta_i)}{\left[(k\sin\theta_i)^2-\left(\frac{\chi'_{vu}}{a_{\mathbf{II}}}\right)^2\right]}\right|^2\right.$$
$$\left.+\left|\sum_{v=-\infty}^{\infty}\sum_{u=1}^{N_{\mathbf{II}}}e^{iv\phi}e^{-i\left(\frac{v}{2}\right)\pi}\begin{pmatrix}\mathbf{\Omega}_m^v\left(u\right)\omega\beta_{vu}\chi_{vu}J'_v\left(\chi_{vu}\right)\frac{(k\sin\theta_i)}{\left[(k\sin\theta_i)^2-\left(\frac{\chi_{vu}}{a_{\mathbf{II}}}\right)^2\right]}\\+\mathbf{\Omega}_e^v\left(u\right)\omega^2 n_{\mathbf{II}}vJ_v(\chi'_{vu})\frac{1}{(k\sin\theta_i)}\end{pmatrix}J_v\left(ka_{\mathbf{II}}\sin\theta_i\right)\right|^2\right\} \quad (50)$$

3. NUMERICAL COMPUTATIONS AND GA OPTIMIZATION

For numerical calculation from the point of convergence, the limitation of v must be determined as a finite number, not an infinite number. The limit is proportional to the aperture size of the cylinder, and v having a finite range from -11 to 11 is appropriate for the case $a_{\mathbf{II}} = 5\lambda$. When v is determined, the maximum modal order at the aperture $N_{\mathbf{II}}$ is automatically determined by (20). Because of the rapidly convergent series in the equations, the calculation is numerically efficient.

Figure 4 shows the specific structure employed for verification. The monostatic RCS calculation by (49) and (50) for the structure in Figure 4 was evaluated and verified through comparison with a FEKO simulation by the method of moments (MoM). Figure 5 and Figure 6 show the RCS comparison in terms of an incident plane wave, respectively. The results of the proposed solution agreed well with the MoM simulated results for θ_i range from 0° to 35°, while a slight error occurred with the proposed solution for θ_i range more than 35°. The reason of the error was using a pair of an incidence and reflected plane wave, as discussed above. The reflected plane wave by the virtual PEC plate were assumed to apply the mode-matching method to the aperture. The assumed PEC plate improperly converted a rim edge into a 90° half-plane wedge, and resulted in an error which was proportional to the θ_i. For a small θ_i, the scattered field by the inside of the circular waveguide cavity is dominant in comparison with an edge diffracted field, therefore the error due to the edge is negligible value. In contrast, the effect of the edge diffraction is noticeable for θ_i more than 35°, thus an accuracy of the proposed solution gradually decrease with increasing θ_i. The proposed solution provides correct analysis of a RCS for an strong JEM effect occur with θ_i range from 0° to 30°. In order to analyze the RCS for an weak JEM effect occur with θ_i more than 30°, the rim edge diffraction must be supplementary considered for accuracy.

For improved reduction of the RCS, the structure of the corrugations requires optimization. We applied GA optimization to the number and unit cell shape of the corrugations. A cost function was defined as

$$f = \left|\mathbf{s}^T\left[\left(R_o^{(1)}\left(\Psi^{(1)}-I\right)+X^{(1)}\left(\Psi^{(1)}+I\right)\right)^{-1}\right]\mathbf{s}\right| \quad (51)$$

where $\mathbf{s} = [1, 1, \ldots, 1]^T$.

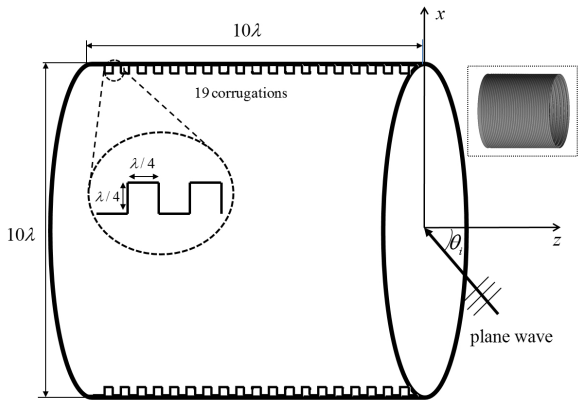

Figure 4. Verification design of the open-ended circular waveguide cavity with corrugations.

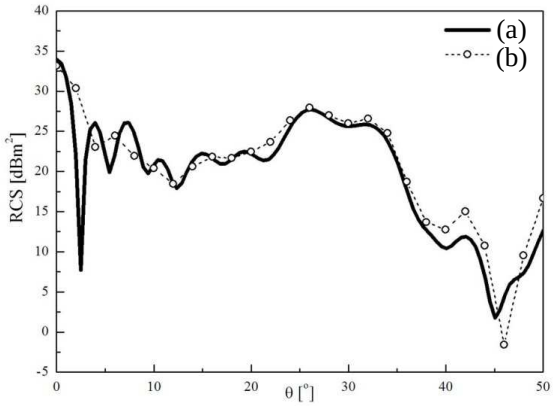

Figure 5. θ-θ pol. RCS of the open-ended corrugated circular waveguide in Figure 4. (a) RCS calculated by the mode-matching and scattering matrix. (b) Simulated result by the MoM.

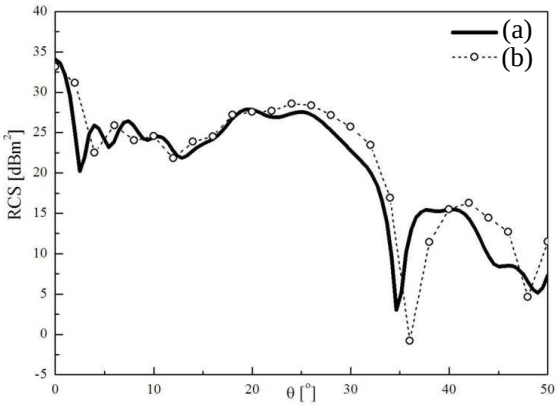

Figure 6. ϕ-ϕ pol. RCS of the open-ended corrugated circular waveguide in Figure 4. (a) RCS calculated by the mode-matching and scattering matrix. (b) Simulated result by the MoM (FEKO).

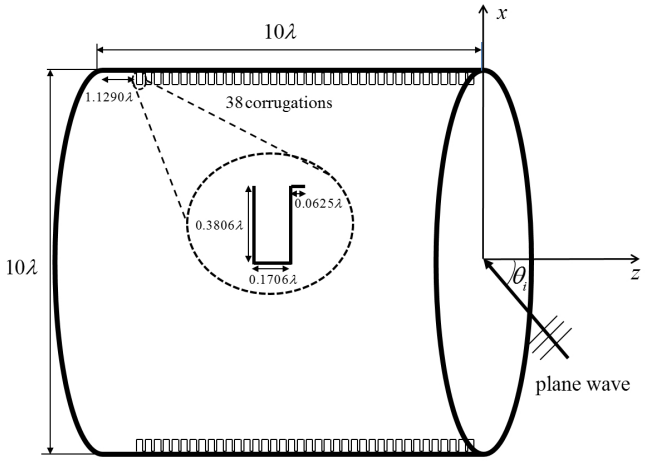

Figure 7. Optimized design of the circular waveguide cavity with corrugations.

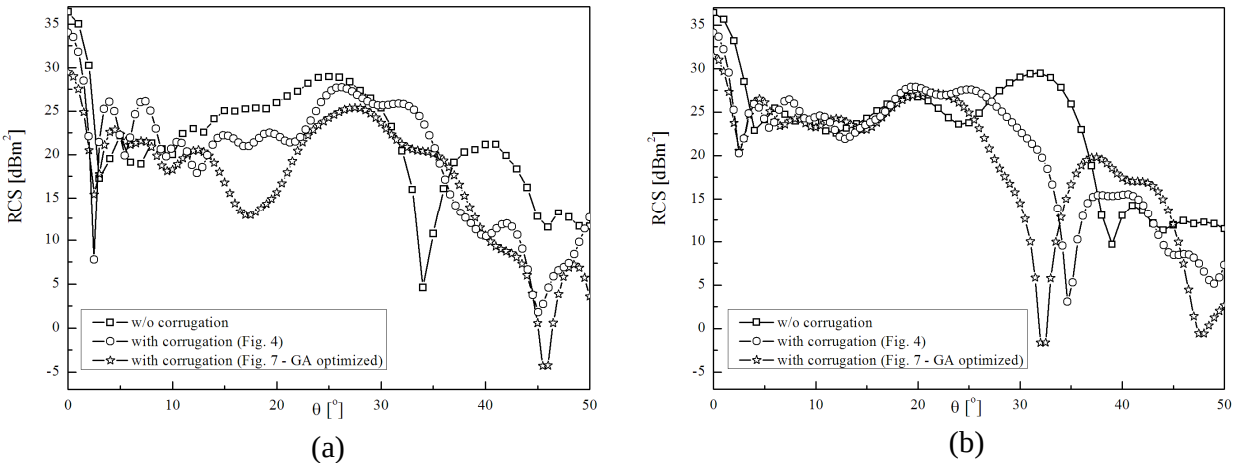

Figure 8. RCS comparison among the three structures. (a) θ-θ pol. (b) ϕ-ϕ pol.

The cost function is proportional to the sum of the modal coefficients (45) at the aperture, and only the dominant order of $v = 1$ is used for convenience. The reduction of the cost function leads to reduction of the scattered wave intensity. Utilizing the GA to minimize the cost function, we obtained the optimized design of the corrugations for the RCS reduction, as shown in Figure 7.

Figure 8 shows the RCS comparison results among the three structures. The first is the non-corrugated circular waveguide cavity with $a_{\mathbf{II}} = 5\lambda$. The second is the circular waveguide cavity with non-optimized corrugations in Figure 4. The third is the circular waveguide cavity with optimized corrugations using GA in Figure 7. The RCS results of all structure were evaluated by the proposed solution (49) and (50). Finally, we confirmed that the RCS is reduced by adding the corrugations to the jet engine inlet.

4. CONCLUSION

For the first time, we analyzed the RCS of the open-ended circular waveguide cavity with corrugations by using mode-matching and scattering matrix methods. We validated the suggested RCS solution with a MoM simulation. The suggested solution with a scattering matrix analysis can be applied to an arbitrary corrugated structure. The suggested modal solution with rapidly converging series also provides computational efficiency. Using these two characteristics, we applied the GA to reconfigure the shape of the corrugations to reduce the RCS. Finally, we obtained the optimized design of the corrugations. The optimized design led to improved RCS reduction. In future work, we will select the best optimization algorithm, variables and cost function for advanced reduction of the jet engine RCS.

APPENDIX A. APPLYING POWER ORTHOGONALITY TO THE BOUNDARY CONDITIONS

$$\begin{aligned}
&\sum_{u=1}^{N_{\mathbf{II}}}\left[\mathbf{A}_{\mathbf{II}}^{(v)}(u)+\mathbf{B}_{\mathbf{II}}^{(v)}(u)\right]\int_0^{a_{\mathbf{II}}}\begin{pmatrix}\bar{e}_m^{\mathbf{II}(v)}(u)\times\bar{h}_m^{\mathbf{III}(v)*}(\zeta)+\bar{e}_e^{\mathbf{II}(v)}(u)\times\bar{h}_m^{\mathbf{III}(v)*}(\zeta)\\+\bar{e}_m^{\mathbf{II}(v)}(u)\times\bar{h}_e^{\mathbf{III}(v)*}(\zeta)+\bar{e}_e^{\mathbf{II}(v)}(u)\times\bar{h}_e^{\mathbf{III}(v)*}(\zeta)\end{pmatrix}\cdot d\bar{s}\\
&=\int_0^{\infty}B_{\mathbf{III}}^{(v)}(\zeta)\int_0^{a_{\mathbf{II}}}\begin{pmatrix}\bar{e}_m^{\mathbf{III}(v)}(\zeta)\times\bar{h}_m^{\mathbf{III}(v)*}(\zeta)+\bar{e}_e^{\mathbf{III}(v)}(\zeta)\times\bar{h}_m^{\mathbf{III}(v)*}(\zeta)\\+\bar{e}_m^{\mathbf{III}(v)}(\zeta)\times\bar{h}_e^{\mathbf{III}(v)*}(\zeta)+\bar{e}_e^{\mathbf{III}(v)}(\zeta)\times\bar{h}_e^{\mathbf{III}(v)*}(\zeta)\end{pmatrix}\cdot d\bar{s}d\zeta\\
&\quad+\int_0^{\infty}\int_0^{a_{\mathbf{II}}}\begin{pmatrix}\left(\bar{E}^i+\bar{E}^r\right)_{\mathrm{TM,TE}}^{(v)}\times\bar{h}_m^{\mathbf{III}(v)*}\\+\left(\bar{E}^i+\bar{E}^r\right)_{\mathrm{TM,TE}}^{(v)}\times\bar{h}_e^{\mathbf{III}(v)*}\end{pmatrix}\cdot d\bar{s}d\zeta
\end{aligned}\tag{A1}$$

$$\begin{aligned}
&\sum_{u=1}^{N_{\mathbf{II}}}\left[\mathbf{B}_{\mathbf{II}}^{(v)}(u)-\mathbf{A}_{\mathbf{II}}^{(v)}(u)\right]\int_0^{a_{\mathbf{II}}}\begin{pmatrix}\bar{h}_m^{\mathbf{II}(v)}(u)\times\bar{e}_m^{\mathbf{II}(v)*}(u)+\bar{h}_e^{\mathbf{II}(v)}(u)\times\bar{e}_m^{\mathbf{II}(v)*}(u)\\+\bar{h}_m^{\mathbf{II}(v)}(u)\times\bar{e}_e^{\mathbf{II}(v)*}(u)+\bar{h}_e^{\mathbf{II}(v)}(u)\times\bar{e}_e^{\mathbf{II}(v)*}(u)\end{pmatrix}\cdot d\bar{s}\\
&=\int_0^{\infty}B_{\mathbf{III}}^{(v)}(\zeta)\int_0^{a_{\mathbf{II}}}\begin{pmatrix}\bar{h}_m^{\mathbf{III}(v)}(\zeta)\times\bar{e}_m^{\mathbf{II}(v)*}(u)+\bar{h}_e^{\mathbf{III}(v)}(\zeta)\times\bar{e}_m^{\mathbf{II}(v)*}(u)\\+\bar{h}_m^{\mathbf{III}(v)}(\zeta)\times\bar{e}_e^{\mathbf{II}(v)*}(u)+\bar{h}_e^{\mathbf{III}(v)}(\zeta)\times\bar{e}_e^{\mathbf{II}(v)*}(u)\end{pmatrix}\cdot d\bar{s}d\zeta\\
&\quad+\int_0^{\infty}\int_0^{a_{\mathbf{II}}}\begin{pmatrix}\left(\bar{H}^i+\bar{H}^r\right)_{\mathrm{TM,TE}}^{(v)}\times\bar{e}_m^{\mathbf{II}(v)*}\\\left(\bar{H}^i+\bar{H}^r\right)_{\mathrm{TM,TE}}^{(v)}\times\bar{e}_e^{\mathbf{II}(v)*}\end{pmatrix}\cdot d\bar{s}d\zeta
\end{aligned}\tag{A2}$$

$$P_o^{(v)}=\begin{pmatrix}-i\omega n_{\mathbf{III}}\beta_{vu}\chi_{vu}J_v'(\chi_{vu})\frac{\zeta^2J_v(\zeta b)}{\zeta^2-\left(\frac{\chi_{vu}}{b}\right)^2} & -\omega^2n_{\mathbf{II}}n_{\mathbf{III}}(iv)J_v(\chi_{vu}')J_v(\zeta b)\\0 & i\omega n_{\mathbf{II}}\frac{\chi_{vu}'^2}{b}J_v(\chi_{vu}')\frac{\kappa_{\mathbf{III}}^*\zeta J_v'(\zeta b)}{\zeta^2-\left(\frac{\chi_{vu}'}{b}\right)^2}\end{pmatrix}\tag{A3}$$

$$Q_o^{(v)}=\begin{pmatrix}-i\omega n_{\mathbf{III}}\kappa_3\zeta & 0\\0 & -i\omega n_{\mathbf{III}}\kappa_{\mathbf{III}}^*\zeta\end{pmatrix}\delta(\zeta-\zeta')\tag{A4}$$

$$R_o^{(v)}=\begin{pmatrix}-\frac{i}{2}\omega n_{\mathbf{II}}\beta_{vu}^*\chi_{vu}^2\left[J_v'(\chi_{vu})\right]^2 & 0\\0 & -\frac{i}{2}\omega n_{\mathbf{II}}\beta_{vu}'\left(\chi_{vu}'^2-v^2\right)\left[J_v(\chi_{vu}')\right]^2\end{pmatrix}\tag{A5}$$

$$\mathbf{V}_{\mathrm{TE}}^{(v)}=\begin{pmatrix}0\\ -2i^v\cos\theta_i\omega n_{\mathbf{II}}\frac{\chi'^2_{vu}}{a_{\mathbf{II}}}J_v(\chi'_{vu})\frac{J'_v(k_{\mathbf{III}}a_{\mathbf{II}}\sin\theta_i)}{(k_{\mathbf{III}}\sin\theta_i)^2-\left(\frac{\chi'_{vu}}{a_{\mathbf{II}}}\right)^2}\end{pmatrix} \tag{A6a}$$

$$\mathbf{V}_{\mathrm{TM}}^{(v)}=\begin{pmatrix}2i^v\beta_{vu}\chi_{vu}k_3\sin\theta_iJ'_v(\chi_{vu})\frac{J'_v(k_{\mathbf{III}}a_{\mathbf{II}}\sin\theta_i)}{(k_{\mathbf{III}}\sin\theta_i)^2-\left(\frac{\chi_{vu}}{a}\right)^2}\\ 2i^v\frac{\omega n_{\mathbf{II}}v}{k_{\mathbf{III}}\sin\theta_i}J_v(\chi'_{vu})J_v(k_{\mathbf{III}}a_{\mathbf{II}}\sin\theta_i)\end{pmatrix} \tag{A6b}$$

$$X^{(v)}=\int_0^\infty\left(P_o^{(v)}\right)^H\left(Q_o^{(v)}\right)^{-1}P_o^{(v)}\,d\zeta=\begin{pmatrix}X^{11}&X^{12}\\X^{21}&X^{22}\end{pmatrix} \tag{A7a}$$

$$X_{mn}^{11}=\int_0^\infty\frac{i\omega n_{\mathbf{III}}\beta^*_{vn}\beta_{vm}\chi_{vm}\chi_{vn}J'_v(\chi_{vm})J'_v(\chi_{vn})\zeta^3\left[J_v\left(\zeta b\right)\right]^2}{\kappa_{\mathbf{III}}\left[\zeta^2-\left(\frac{\chi_{vm}}{b}\right)^2\right]\left[\zeta^2-\left(\frac{\chi_{vn}}{b}\right)^2\right]}d\zeta \tag{A7b}$$

$$X_{mn}^{12}=\int_0^\infty\frac{i\omega^2n_{\mathbf{II}}n_{\mathbf{III}}v\beta^*_{vn}\chi_{vn}J_v(\chi'_{vm})J'_v(\chi_{vn})\zeta\left[J_v\left(\zeta b\right)\right]^2}{\kappa_{\mathbf{III}}\left[\zeta^2-\left(\frac{\chi_{vn}}{b}\right)^2\right]}d\zeta \tag{A7c}$$

$$X_{mn}^{21}=\int_0^\infty\frac{i\omega^2n_{\mathbf{II}}n_{\mathbf{III}}v\beta_{vm}\chi_{vm}J_v(\chi'_{vn})J'_v(\chi_{vm})\zeta\left[J_v\left(\zeta b\right)\right]^2}{\kappa_{\mathbf{III}}\left[\zeta^2-\left(\frac{\chi_{vm}}{b}\right)^2\right]}d\zeta \tag{A7d}$$

$$\begin{aligned}X_{mn}^{22}=&\int_0^\infty\frac{i\omega^3n_{\mathbf{II}}^2n_{\mathbf{III}}v^2J_v(\chi'_{vm})J_v(\chi'_{vn})\left[J_v(\zeta a_{\mathbf{II}})\right]^2}{\kappa_{\mathbf{III}}\zeta}d\zeta\\&+\int_0^\infty\frac{i\omega\frac{n_{\mathbf{II}}^2}{n_{\mathbf{III}}}\left(\frac{\chi'_{vm}\chi'_{vn}}{a_{\mathbf{II}}}\right)^2J_v(\chi'_{vm})J_v(\chi'_{vn})\kappa_{\mathbf{III}}\zeta\left[J'_v\left(\zeta a_{\mathbf{II}}\right)\right]^2}{\left[\zeta^2-\left(\frac{\chi'_{vm}}{a_{\mathbf{II}}}\right)^2\right]\left[\zeta^2-\left(\frac{\chi'_{vn}}{a_{\mathbf{II}}}\right)^2\right]}d\zeta\end{aligned} \tag{A7e}$$

APPENDIX B. P, Q, R MATRICES FOR SCATTERING MATRIX ANALYSIS

$$P^{(v)}=\begin{pmatrix}P^{11}&P^{12}\\0&P^{22}\end{pmatrix} \tag{B1a}$$

$$P_{mn}^{11}=i\omega n_{\mathbf{II}}\beta_{vm}\frac{\chi_{vm}}{a}\frac{\chi_{vn}}{b}\frac{\frac{a}{b}\chi_{vn}J'_v\left(\chi_{vm}\right)J_v\left(\frac{a}{b}\chi_{vn}\right)}{\left(\frac{\chi_{vm}}{a}\right)^2-\left(\frac{\chi_{vn}}{b}\right)^2} \tag{B1b}$$

$$P_{mn}^{12}=-\omega^2n_{\mathbf{I}}n_{\mathbf{II}}(iv)J_v(\chi'_{vm})J_v\left(\frac{a}{b}\chi_{vn}\right) \tag{B1c}$$

$$P_{mn}^{22}=-i\omega n_{\mathbf{I}}\beta'^*_{vn}\frac{\chi'_{vm}\chi'_{vn}}{ab}\frac{\chi'_{vm}J_v\left(\chi'_{vm}\right)J'_v\left(\frac{a}{b}\chi'_{vn}\right)}{\left(\frac{\chi'_{vm}}{a}\right)^2-\left(\frac{\chi'_{vn}}{b}\right)^2} \tag{B1d}$$

$$Q^{(v)}=\begin{pmatrix}Q^{11}&0\\0&Q^{22}\end{pmatrix} \tag{B2a}$$

$$Q^{11}=\mathrm{diag}\left[-\frac{i}{2}\omega n_{\mathbf{II}}\beta_{vn}\chi_{vn}^2\left[J'_v(\chi_{vn})\right]^2\right] \tag{B2b}$$

$$Q^{22}=\mathrm{diag}\left[-\frac{i}{2}\omega n_{\mathbf{II}}\beta'^*_{vn}\left(\chi'^2_{vn}-v^2\right)\left[J_v(\chi'_{vn})\right]^2\right] \tag{B2c}$$

$$R^{(v)}=\begin{pmatrix}R^{11}&0\\0&R^{22}\end{pmatrix} \tag{B3a}$$

$$R^{11}=\mathrm{diag}\left[-\frac{i}{2}\omega n_1\beta^*_{vm}\chi_{vm}^2\left[J'_v(\chi_{vm})\right]^2\right] \tag{B3b}$$

$$R^{22}=\mathrm{diag}\left[-\frac{i}{2}\omega n_{\mathbf{I}}\beta'_{vm}\left(\chi'^2_{vm}-v^2\right)\left[J_v(\chi'_{vm})\right]^2\right] \tag{B3c}$$

REFERENCES

1. Bell, M. R. and R. A. Grubbs, "JEM modeling and measurement for radar target identification," *IEEE Trans. Aerospace and Electronic Systems*, Vol. 29, No. 1, 73–87, Jan. 1993.
2. Anastassiu, H. T., "Electromagnetic scattering from simple jet engine models," *IEEE Transactions on Antennas and Propagation*, Vol. 44, No. 3, 420–421, 1996
3. Altintas, A., P. H. Pathak, and M.-C. Liang, "A selective modal scheme for the analysis of EM coupling into or radiation from large open-ended waveguides," *IEEE Transactions on Antennas and Propagation* Vol. 36, No. 1, 84–96, 1988.
4. Chan, K. K. and S. Wong, "Accurate RCS prediction of electrically large jet inlets and engines," *IEEE International Conference on Antennas and Propagation*, Vol. 1, No. 491, 253–256, 2003.
5. Chan, K. K., S. K. Wong, and E. S. Riseborough, "Radar cross section modeling and measurements of inlets and cylinders with skew blades," *IEEE Transactions on Antennas and Propagation*, Vol. 54, No. 10, 2930–2939, 2006.
6. Bourlier, C., H. He, J. Chauveau, R. Hémon, and P. Pouliguen, "RCS of large bent waveguide ducts from a modal analysis combined with the Kirchhoff approximation," *Progress In Electromagnetics Research*, Vol. 88, 1–38, 2008
7. Hao, L., R.-C. Chou, and S.-W. Lee, "Shooting and bouncing rays: Calculating the RCS of an arbitrarily shaped cavity," *IEEE Transactions on Antennas and Propagation*, Vol. 37, No. 2, 194–205, 1989.
8. Lee, C. and S.-W. Lee, "RCS of a coated circular waveguide terminated by a perfect conductor," *IEEE Transactions on Antennas and Propagation*, Vol. 35, No. 4, 391–398, 1987.
9. Burkholder, R. J., "A fast and rapidly convergent iterative physical optics algorithm for computing the RCS of open-ended cavities," *Applied Computational Electromagnetics Society Journal*, Vol. 16, No. 1, 53–60, 2001.
10. Garcia-Pino, A., F. Obelleiro, and J. L. Rodriguez, "Scattering from conducting open cavities by generalized ray expansion (GRE)," *IEEE Transactions on Antennas and Propagation,* Vol. 41, No. 7, 989–992, 1993.
11. Anastassiu, H. T., J. L. Volakis, and D. S. Filipovic, "Integral equation modeling of cylindrically periodic scatterers in the interior of a cylindrical waveguide," *IEEE Transactions on Microwave Theory and Techniques*, Vol. 46, No. 11, 1713–1720, 1998.
12. Barka, A. and N. Douchin, "Asymptotic simplifications for hybrid BEM/GO/PO/PTD techniques based on a Generalized Scattering Matrix approach," *Computer Physics Communications*, Vol. 183, No. 9, 1928–1936, 2012.
13. Kusiek, A. and J.Mazur, "Analysis of scattering from arbitrary configuration of cylindrical objects using hybrid finite-difference mode-matching method," *Progress In Electromagnetics Research*, Vol. 97, 105–127, 2009.
14. Lim, H. and N.-H. Myung, "A novel hybrid AIPO-MoM technique for jet engine modulation analysis," *Progress In Electromagnetics Research*, Vol. 104, 85–97, 2010.
15. Chou, R.-C. and S.-W. Lee, "Modal attenuation in multilayered coated waveguides," *IEEE Transactions on Microwave Theory and Techniques*, Vol. 36, No. 7, 1167–1176, 1988.
16. Mosallaei, H. and Y. Rahmat-Samii, "RCS reduction of canonical targets using genetic algorithm synthesized RAM," *IEEE Transactions on Antennas and Propagation,* Vol. 48, No. 10, 1594–1606, 2000.
17. Chen, H. T., G.-Q. Zhu, and S.-Y. He, "Using genetic algorithm to reduce the radar cross section of three-dimensional anisotropic impedance object," *Progress In Electromagnetics Research B*, Vol. 9, 231–248, 2008.
18. Lee, H. S. and H. J. Eom, "Electromagnetic scattering from a thick circular aperture," *IEEE Transactions on Microwave and Optical Technology Letters*, Vol. 36, No. 3, 228–231, 2003.
19. Lee, H. S. and H. J. Eom, "Scattering from a cylindrical waveguide with rectangular corrugations," *IEEE Transactions on Microwave Theory and Techniques*, Vol. 49, No. 2, 315–320, 2001.

20. Eleftheriades, G. V., "Some important properties of waveguide junction generalized scattering matrices in the context of the mode matching technique," *IEEE Transactions on Microwave Theory and Techniques*, Vol. 42, No. 10, 1896–1903, 1994.
21. Park, Y. B. and H. J. Eom, "Electromagnetic transmission through multiple circular apertures in a thick conducting plane," *IEEE Transactions on Antennas and Propagation*, Vol. 52, No. 4, 1049–1055, 2004.
22. Shampine, L. F., "Vectorized Adaptive Quadrature in MATLAB," *Journal of Computational and Applied Mathematics*, Vol. 211, 131–140, 2008.